Delayed collapse transitions in a pinned polymer system

Keerti Chauhan* and Ankit Singh
Department of Physics, Banaras Hindu University, Varanasi 221005, India

(Received 11 April 2022; revised 27 May 2022; accepted 5 June 2022; published 27 June 2022)

Employing Langevin dynamics simulations, we investigated the kinetics of the collapse transition for a polymer of length N when a particular monomer at a position $1 \leqslant X \leqslant N$ is pinned. The results are compared with the kinetics of a free polymer. The equilibrium θ-point separating the coil from the globule phase is located by a crossover in $\langle R_g^2 \rangle / N$ plots of different chain lengths. Our simulation supports a three-stage mechanism for free and pinned polymer collapse: the formation of pearls, the coarsening of pearls, and the formation of a compact globule. Pinning the central monomer has negligible effects on the kinetics as it does not break the symmetry. However, pinning a monomer elsewhere causes the process to be delayed by a constant factor ϕ_X depending linearly upon X. The total collapse time scales with N as $\tau_c \sim \phi_X N^{1.60 \pm 0.03}$, which implies τ_c is maximum when an end monomer is pinned ($X = 1$ or N), while when pinning the central monomer ($X = N/2$) it is minimum and identical to that of a free polymer. The average cluster size $N_c(t)$ grows in time as t^z, where $z = 1.00 \pm 0.04$ for a free particle, whereas we identify two time regimes separated by a plateau for pinned polymers. At longer times, $z = 1.00 \pm 0.04$, while it deviates in early time regimes significantly, depending on the value of X.

DOI: 10.1103/PhysRevE.105.064505

I. INTRODUCTION

The dynamics of a coil-globule transition in a polymer system, when the solvent conditions are changed from "good" to "poor" [1], has been of great interest since the first study of Stockmayer [2]. In the good solvent, the chain remains swollen and the radius of gyration scales with the degree of polymerization as $R_g \sim N^{3/5}$. When the solvent changes from good to poor, scaling is found as $R_g \sim N^{1/3}$ [1–3]. Generally, the solvent conditions are determined by an interplay between the monomer-monomer, monomer-solvent, and solvent-solvent interactions, and they can be changed upon variation of the system's properties, e.g., temperature, pH, interactions, etc. For example, in a low-temperature regime, monomer-monomer interaction is strong, which favors the globule state, while at higher temperatures, the magnitude of this interaction is insufficient to perturb the coil state conformation. For the continuous drop in temperature from a higher to a lower range, the transition can be located, and it is the so-called θ-point, where the polymer behaves as an ideal chain as $R_g \sim N^{1/2}$ and the associated temperature is called the θ-temperature.

de Gennes and co-workers proposed the first theoretical study of the coil-to-globule transition dynamics [4]. They proposed an "expanding sausage model," i.e., a two-stage model in which the collapsing of a random-coil linear chain leads to crumple (or blob) formation on a minimal scale along the chain backbone. After that, the blobs that absorb monomers form bigger blobs until a compact globule is formed [4,5]. The associated characteristic relaxation times τ_{crumple} and τ_{collapse} are measured experimentally, showing that crumpling happens faster while collapsing is slower [6]. Later, Halperin and Goldbart proposed a three-stage "pearl necklace model" in which the blobs grow in size by absorbing the beads from the bridges connecting them until the bridges become straightened, which makes the polymer conformation look like a "pearl necklace," and finally the clusters join together and deform into a globule. They also proposed three characteristic times corresponding to the three different stages, i.e., scale as N^0, $N^{1/5}$, and $N^{6/5}$, respectively [7]. Several studies using Langevin models [8,9], phenomenological models [5,10], and computer simulations [11–14] have been used to consider the kinetics of collapse in the absence of topological constraints; however, there is no consensus on the exact mechanisms and scaling law for these stages ("pearling," bridge-stretching, and collapse).

For a free polymer, Flory first predicted that the scaling between the characteristic collapse time and N should follow the relation $\tau_c \sim N^2$ [3]. Later, Pham *et al.* obtained a relation $\tau_c \sim N^{1.01}$ using Brownian dynamics simulations [15]. The collapse time is proposed to scale as $\tau_c \sim N^{0.93}$ in Ref. [10], $\tau_c \sim N^{4/3}$ in Refs. [16,17], and $\tau_c \sim N^{0.98}$ as reported by Guo using the dissipative particle dynamics simulations [18]. The increase in the collapse times with increasing chain length is an expected result as it depends on how fast smaller blobs absorb others to form the final compact structure [7,15,19–24]. In a free polymer, the crumpling and coarsening process starts from both ends and leads to the globule formation at the center. Studies related to the kinetics of a collapsing polymer with constraints, such as anchored polymers near wedges and surfaces [25–28], have incorporated the effect of perturbed symmetry due to pinning the chain to the surface. While the impact of topological constraints on the equilibrium

*keertichauhan1234@gmail.com

properties of the polymer have been widely explored, kinetic studies of such systems remain elusive. Particularly in the context of polymer aggregation, the constraint's effect on the characteristic times of various stages involved, such as the local blob formation and coarsening, can reveal some intriguing results.

The method of pinning a fraction of a particle by completely freezing the degree of freedom and observing the thermodynamics of the remaining free particles has been successfully applied to determine the existence of static cooperative lengthscales in numerical models [29,30]. For example, in glass-forming liquids, pinning induces a new kind of glass transition, namely the random pinning glass transition (RPGT) [31,32], which can be used to predict some features of standard thermodynamic glass transitions [33,34]. While pinning methods have been widely used to showcase studies on the diverse class of systems such as molecular liquids, magnetic spin systems, and glass systems [29–31,35–37], only a few studies are available related to equilibrium and kinetic studies on pinned polymer systems [28,38–40].

Since molecules are connected through a finitely extensible string, in this case of a polymer, pinning random sites or fractions may not be as applicable as in a free-particle system. However, moving the position of an arbitrarily pinned monomer can provide better insight into various stages involved in the transition process. Polymer translocation through an interacting pore is one such exciting example. In experiments, it is found that the blockade current mainly depends on the few nucleotides passing through the channel at a time in the threading process. The monomer at the interface interacts with the pore. It divides the chain into two unequal lengths across the pore, allowing the polymer to achieve different configurations on two sides [41]. The effect of unequal entropy can be seen in the calculated mean first passage times and the free-energy profile of a translocating polymer. In case the solvent conditions felt by the polymer across the pore are not similar, it is found that the translocation time depends on the time of globule formation as well as the size of the globule on the other side [42,43].

The paper is organized as follows: In Sec. II, we briefly discuss the model and describe the Langevin equation used to obtain the thermodynamic parameters of interest. In Sec. III, we locate the θ-point for the coil-globule transition by calculating equilibrium values of $\langle R_g \rangle$ at different temperatures. Section IV deals with the kinetics of transition, when the polymer is pushed into a globule state condition from the extended state with variable pinning positions of a monomer. The collapse time of the process as a parameter of length and pinning index is investigated in Sec. V. Finally, we present a brief discussion in Sec. VI.

II. MODEL AND METHOD

We consider a simple coarse-grained model of a linear polymer chain (see Fig. 1), and we impose restrictive interaction among monomers, which is sufficient to capture some essential properties of different biopolymers, as explained in Refs. [24,44]. The energy of the system is defined

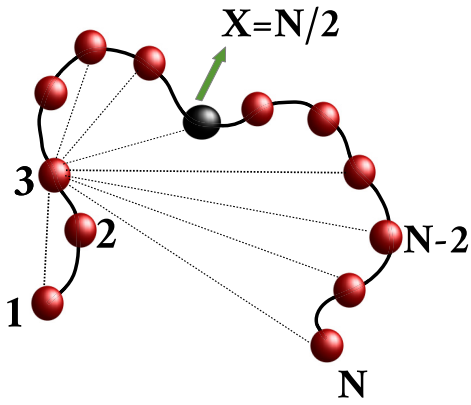

FIG. 1. Schematic representations of a self-interacting polymer with a pinned monomer. The monomer presented with the black sphere is pinned, and the other monomers are free to configure in the space. X indicates the position of the pinned monomer, and $X = N/2$ represents a specific case in which the central monomer is pinned. Here, every monomer can interact with the rest of the (nonadjacent) monomers of the chain. The dashed lines show the attractive interaction among the third and other nonbonded monomers.

as

$$E = \sum_{i=1}^{N-1} \frac{K}{2}(d_{i,i+1} - d_0)^2 + \sum_{i=1}^{N-1} \sum_{j \geqslant i+1}^{N} 4\epsilon \left[\left(\frac{\sigma}{d_{i,j}} \right)^{12} - \left(\frac{\sigma}{d_{i,j}} \right)^{6} \right], \tag{1}$$

where $d_{i,j} = |\vec{r}_i - \vec{r}_j|$ denotes the distance between the ith and jth bead, $\vec{r}_i$ is the position of the ith monomer, and the number of monomers is denoted by N. The adjacent monomers are connected with a harmonic spring, and the potential between them is explained by the first term in the above equation. The nonbonded monomers interact via the Lennard-Jones (LJ) potential, shown as the second term in Eq. (1) with the interaction strength $\epsilon = 1$. Following Refs. [24,44], we set the equilibrium distance in the harmonic potential as $d_0(= 1)$ and $k\sigma^2/\epsilon = 34$, where σ is the unit for distance measurements.

The Langevin equation can provide a complete description of the collapse on all timescales and thus allows for a systematic analysis of the problem. The following stochastic differential equation, which includes friction and noise terms, is used to obtained the time evolution of the system:

$$m\frac{d^2\boldsymbol{r}}{dt^2} = -\zeta\frac{d\boldsymbol{r}}{dt} + \boldsymbol{F}_c + \boldsymbol{\Gamma}, \tag{2}$$

where m is the mass, $\zeta = 0.4m/\tau$ is the friction coefficient, and $\boldsymbol{\Gamma}$ is random force with zero mean [44–46]. $\boldsymbol{F}_c = -\nabla H$ is the conservative force and $\boldsymbol{\Gamma}$ is the white noise, which is related to the friction coefficient by the fluctuation dissipation theorem $\langle \Gamma_i(t)\Gamma_j(t')\rangle = 2\zeta k_B T \delta_{i,j}\delta(t - t')$. The temperature (T) is measured in units of ϵ/k_B, where k_B is the Boltzmann constant, and $\delta(t - t')$ is the Dirac δ-function. To incorporate this numerically, we use the sixth-order Gear algorithm with a time step $\Delta t = 0.005\tau$, where $\tau \equiv \sqrt{m\sigma^2/\epsilon}$. Time is measured in units of τ, and the presented results are averaged over many trajectories.

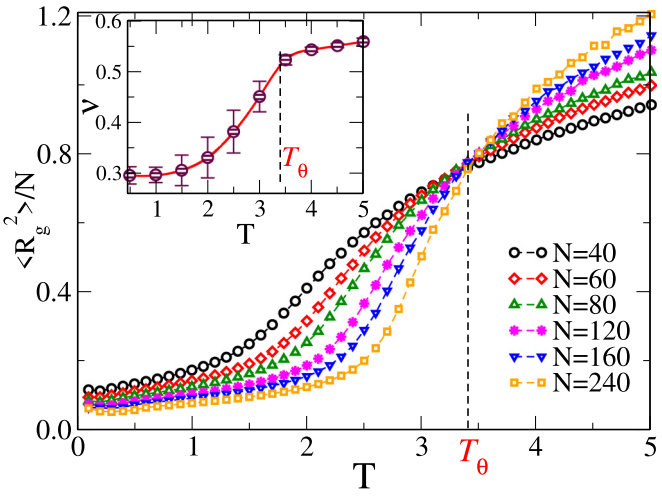

FIG. 2. The scaled mean-square radius of gyration $\langle R_g^2\rangle/N$ as a function of temperature for different chain lengths (from $N = 40$ up to 240). The θ-point is located at $T_\theta = 3.4$. The Flory exponent ν, which is related to R_g with relation $R_g \sim N^\nu$, is shown in the inset, which scales from 0.30 to 0.56 (with the given error bars) and attains a value $\nu = 1/2$ at the θ-point. The markers shows the data point, while the curve represents the least-squares fit.

III. LOCATING THE θ-POINT

As discussed in the Introduction, the point where two phases separate is called the θ-point. At the θ-point, the chain behaves as ideal because the monomer-monomer attraction perfectly balances the excluded volume interaction. The Flory exponent ν, which relates the radius of gyration with N ($R_g \sim N^\nu$), attains a value $\nu = 1/2$, between $\nu = 1/3$ (globule phase) and $\nu = 3/5$ (coil phase). Another quantity, $\langle R_g^2\rangle/N$, behaves independent of the chain length. A crossover in $\langle R_g^2\rangle/N$ versus temperature (T) curve for different N values is used to locate the θ-point here (see Fig. 2).

Depending on temperature values, the polymer can achieve three nontrivial phases: the collapsed phase at low temperatures, the random walk phase (RW) at medium temperatures, and the self-avoiding random walk phase (SARW) at higher temperatures. The transition between the collapsed and RW phases is a phase transition, while a smooth crossover transition separates the RW and SARW phases. To locate the θ-point in our system, we analyzed the values of ν and R_g in a temperature range from *better-than-*θ to *worse-than-*θ only. Lengths varied from a minimum of $N = 40$ up to $N = 240$. We performed a simulation for a time duration of $6 \times 10^8 \Delta t$, and after equilibrium is achieved at $2 \times 10^8 \Delta t$; data are sampled on an interval of Δt for a duration of another $4 \times 10^8 \Delta t$.

In Fig. 2, we plotted $\langle R_g^2\rangle/N$ as a function of temperature for different chain lengths, and we identify the phase transition at the point of intersection. We differentiate a low-temperature phase from a high-temperature phase passing through the θ-point. We found $T_\theta = 3.4$, close to the value reported in Refs. [47–54]. In the inset of Fig. 2, the Flory exponent ν is calculated using the $\langle R_g\rangle$ values, shown in the main plot. At very low temperatures $T < 1$, the value of the Flory coefficient is $\nu = 0.3$, which corresponds to the globule state. A decent rise is registered in the ν curve as the temperature increases until it attains a value $\nu = 0.5$ at the transition temperature $T_\theta = 3.4$. A further increase in temperature yields a saturation in the ν plot at $\nu = 0.56$, which shows that the polymer has finally achieved the coiled state. This value of $T_\theta = 3.4$ and $\langle R_g^2(T_\theta)\rangle/N \sim 0.75$ is used as a reference for further calculations.

IV. KINETICS OF TRANSITION

The transition from the coil to a globule follows the "pearl necklace" mechanism, an effective three-step mechanism. The crumple formation characterizes the first step, sometimes called tiny clusters, blobs or droplets, throughout the chain. The second and third stages correspond to the coarsening and the compact globule formation stage. Crumpling happens faster and collapses relatively slower [6]. Since we aim to understand the collapse of a polymer chain when an arbitrarily chosen monomer is pinned in the chain, we ensure that the polymer initially (at $t = 0$) remains in its stretched state to avoid crumples before the simulation starts. For implementation, we choose a polymer configuration equilibrated in the SARW phase (at a very high temperature) to ensure that monomers do not form any non-native bonds before the process starts. We used the same initial condition for every simulation so that the local blob formation before quenching does not affect the transition's kinetics when the monomer is pinned. The system immediately quenched into poor solvent conditions by abruptly decreasing the temperature below the transition point down to $T = 1.0$ (as $T_\theta = 3.4$ from Fig. 2).

First, we analyze the collapse of a free polymer at varying temperatures. In Figs. 3(a)–3(e), chain configurations show a typical sequence of events along with the folding pathway for a free polymer chain. Initially formed crumples are encircled with dots across the length in the Fig. 3 snapshots. Figure 3(b) shows blobs of increased size after absorbing monomers from the smaller blobs along the bridges between them. The "bridge straightening" stage proposed by Halperin and Goldbart is apparent from Fig. 3(c), where two smaller compact globules are pushing outwards, and the bridge between them is stretching. In the end, bridge monomers are also absorbed by the two globules to form a deformed globule, as shown in Fig. 3(d), which relaxes to a perfect spherical globule state after equilibration, shown with the solid circle in Fig. 3(e).

To study the coil-globule transition in a pinned polymer system, we froze the degree of freedom of an arbitrarily chosen monomer at its equilibrium position. The thermodynamics of the remaining free chain is studied. Pinning an end monomer (when pinning index $X = 1$ or $X = N$), hereby referred to as an anchored polymer, represents the similar dynamics involved in studies related to a polymer anchored to noninteracting wedges or surfaces through fixing the one end only [26,27]. Moving the pinned monomer towards the center partitions it into two chains of unequal lengths. For example, $X = N/2$ indicates that the pinned monomer sits at the center of the chain and divides it into two almost equal parts. This example is also shown in the schematic diagram of the model, Fig. 1, where the pinned monomer is represented by a black sphere, and other free monomers are represented by maroon.

As an aggregate measure of the process, we monitor $\langle R_g\rangle$ as a function of time. The results are shown in Figs. 4 and 5 for a free and pinned polymer, respectively. In the first column

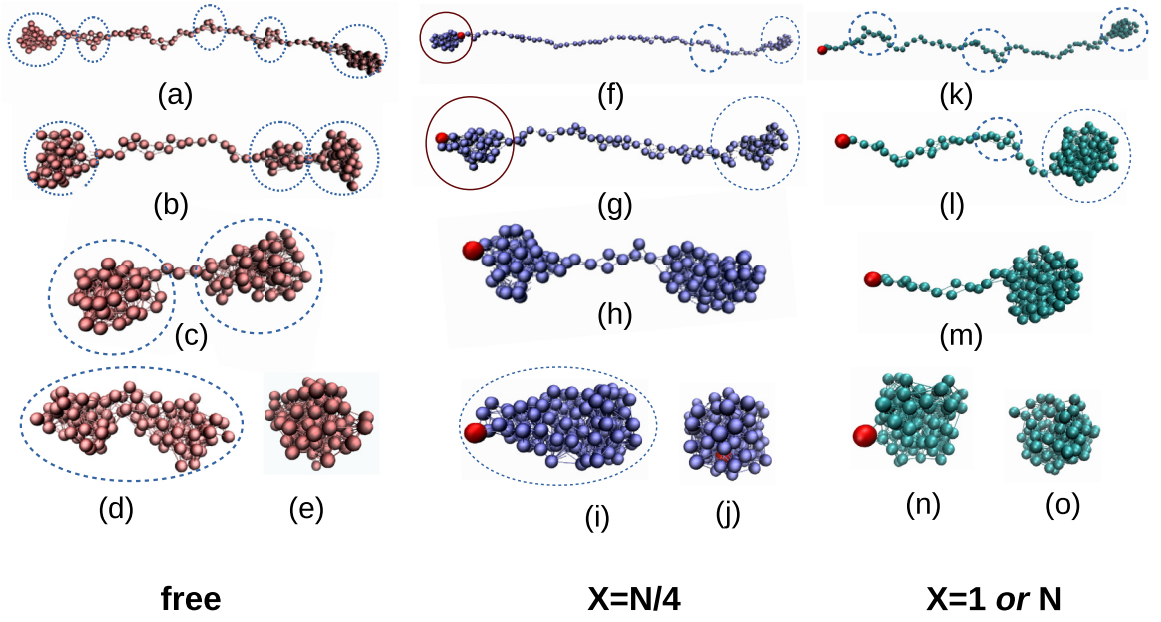

FIG. 3. Pathway of a collapsing polymer at temperature $T = 1.0$ with 120 beads. The red monomer is the pinned monomer. The left panel (a)–(e) represents collapse stages for a free polymer, the midpanel (f)–(j) for $X = N/4$, and the right panel (k)–(o) presents stages for $X = 1$ (the anchored polymer). A dashed circle represents activated globules or crumples, while solid circles show the final structures. In the case of a free polymer, crumpling and coarsening are symmetric at both free ends, while in the second case, $X = N/4$, the chain is divided into two parts of unequal entropy. Fast aggregation of the shorter chain around the pinned monomer is observed before the longer segment could overcome the crumpling process. In the third case of an anchored polymer ($X = 1$), crumpling and coarsening are both biased to start from the free end only.

of Fig. 5, we plotted R_g versus t for (a) anchored: $X = 1$ or $X = N$, (b) $X = N/4$, and (c) $X = N/2$, when the pinned monomer is moved to the chain's one-fourth and half-length, respectively. The effect of increasing length is apparent in Fig. 4, as $\langle R_g \rangle$ relaxes faster for the shorter chains, and slowest for $N = 160$ among all the chain lengths shown in the plot. In Fig. 4 (inset), collapse time is shown, which we will discuss later in the next section.

The pinning effect on $\langle R_g \rangle$ versus t plots is shown for various chain lengths from $N = 40$ up to $N = 160$. In the second column, we analyzed the effect of various pinning sites,

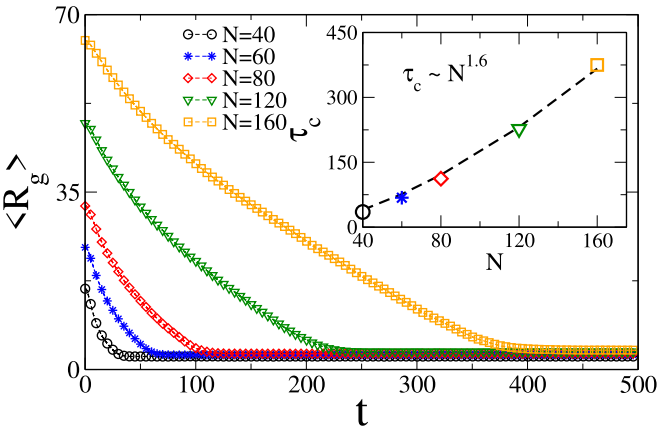

FIG. 4. $\langle R_g(t) \rangle$ vs t for a free polymer of variable chain lengths. The inset shows the dependency of collapse time τ_c, obtained using Eq. (4) (discussed in Sec. V) on N. The markers represent the calculated values, and the curve represents the fit $\tau_c \sim N^{1.60 \pm 0.03}$. The error bars are obtained by using the method of least squares.

keeping the chain length fixed as (a) $N = 40$, (b) $N = 80$, and (c) $N = 120$. By doing so, a comparison of timescales induced by the two parameters [the chain length (N) and the pinning site (X)] can be drawn. For homogeneity between the plot of different lengths (N), plotted in the second column, we introduced a variable n, which is related to X by the relation $X = n \times (N/10)$. For $N = 40$, $n = 1$ to 5 represents $X = 4$, 8, 12, 16, and 20, while for $N = 80$, similar n values represent the corresponding $X = 8$, 16, 24, 32, and 40 values. The presented curves are averaged over 200 trajectories. The curves are all seen to be smooth and monotonic, which means that there is no trapping throughout the process.

From the snapshots in Figs. 3(a)–3(e), we can see that the coarsening process is more effective at the ends of the chain, and small globules are absorbed towards the center. Right before the process ends, two more giant globules are formed containing two ends of the chain, and they merge into a single deformed globule, which relaxes as a perfect spherical globule. This indicates that the collapse is symmetric, and any asymmetry can influence its dynamics. Pinning a monomer at its position $1 \leqslant X \leqslant N$ breaks the symmetry, and now one side has more entropy with respect to another. The configurations of Figs. 3(f)–3(j) in the central panel represent a system where a monomer at $X = N/4$ is pinned, and Figs. 3(k)–3(o) represent the same for an anchored polymer.

Pinning an inner monomer dissects the chain into two parts of unequal lengths. It is evident from Figs. 3(f)–3(j) that for $X = N/4$, coarsening can start from both ends. In fact, at the end, close to the pinned monomer, accumulation starts around the fixed bead very fast. After the globule at the shorter end is formed, it absorbs the monomer from the other segment,

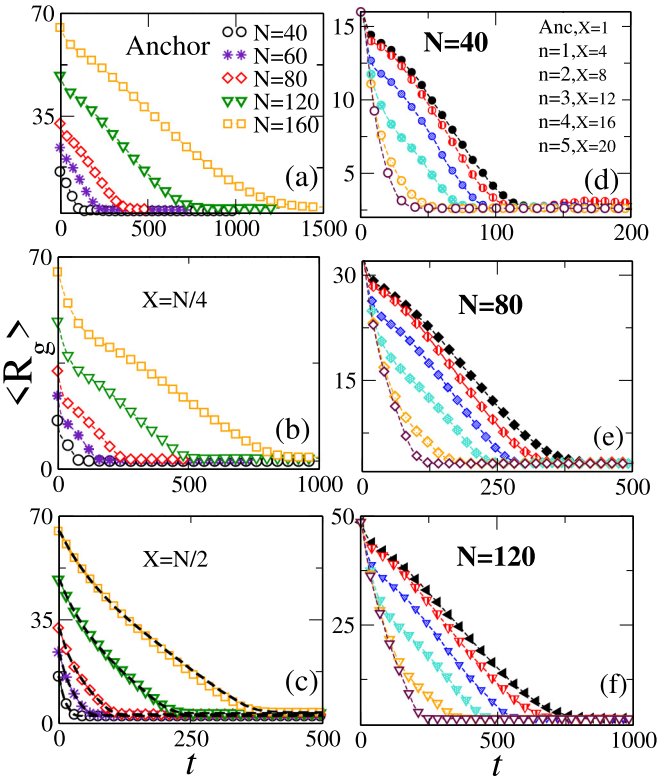

FIG. 5. Plots (a), (b), and (c) represents the dependency of $\langle R_g(t)\rangle$ on time t for the anchored case ($X = 1$), $X = N/4$, and $X = N/2$, respectively, for different chain lengths. The dotted lines in (c) represent data for a free polymer (same as shown in Fig. 4), which indicates that kinetics are identical for both of the systems. Plots (d)–(f) represent the same for fixed N and varying X. Variable n is related with X by the relation $X = n \times N/10$, and the corresponding X values are given along with the n values in plot (d) for length $N = 40$. Each curve is averaged over 200 samples.

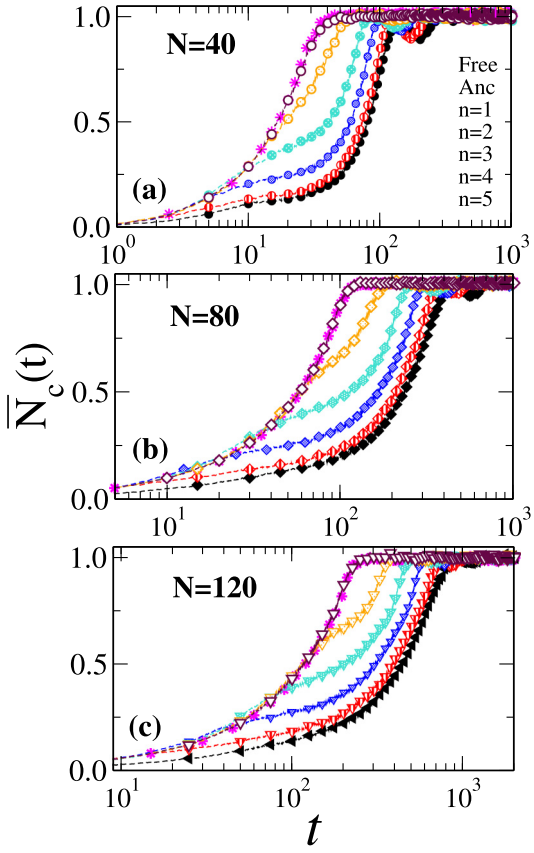

FIG. 6. Normalized average nearest-neighbor contacts per monomer $\bar{N}_c(t)$ vs t [as defined in Eq. (3)] during collapse for various chain lengths (a) $N = 40$, (b) $N = 80$, and (c) $N = 120$. Each panel shows $\bar{N}_c(t)$ vs t plot for different pinning positions, X. X is related with n as described in the caption of Fig. 5 (also refer to the text).

away from the pinned monomer [see Fig. 3(g)]. Later, the remaining two globules form a deformed globule far from the pinned monomer, soon absorbed inside the perfect globule.The pinned monomer is represented as a relatively bigger (red) bead for more explicit identification in Figs. 3(f)–3(o).

In the case of an anchored polymer, Figs. 3(k)–3(o), crumpling can happen anywhere along the chain, but coarsening is now limited to the free end only. It is now visible that the stage where two globules survive until the end vanishes, and a single deformed globule is formed, which fluctuates away from the pinned monomer. Later, the pinned monomer is also absorbed, forming the final spherical globule. It is not surprising that $\langle R_g\rangle$ relaxes slowest for the anchored polymer in Fig. 5(a).

The effect of length can be seen in the plots of the first column of Fig. 5, similar to Fig. 4. The timescales are longer as the chain length increases, visible in all the figures as the collapse of $\langle R_g\rangle$ is fastest for the minimum for $N = 40$ and is maximum for $N = 160$. In the second column of Figs. 5(d)–5(f), the effect of pinning is included. It is apparent from Figs. 5(a)–5(c) that folding kinetics is slowest for an anchored polymer ($X = 1$ or N). As the pinned monomer moves towards the center, the quenching happens faster for all chain lengths. From Fig. 5, one can conclude that $\langle R_g\rangle$ relaxes faster as the system becomes symmetric, and a comparison of dynamical timescales can be drawn for continuous change in the pinning position (X). For example, in case of $N = 160$, $\langle R_g\rangle$ relaxes close to $t = 1500$, which is reduced down to $t = 1000$ in the case of $X = N/4$ [Fig. 5(b)]. In Fig. 5(c), we have plotted $\langle R_g\rangle$ values for a free polymer (dotted lines) and $X = N/2$. By pinning a monomer at $X = N/2$, the system remains symmetric, which resembles the free chain system; the quenching in the two systems is identical and is the fastest.

In Fig. 6, we have plotted the normalized average number of contacts per monomer $[\bar{N}_c(t)]$ as a function of time t for (a) $N = 40$, (b) $N = 80$, and (c) $N = 120$. The monomer creates a contact with the surrounding monomer during collapse when the distance between them, d_{ij}, is less than the cutoff distance d_c. We set the cutoff distance $d_c = 1.50$. Normalization is obtained using the following relation:

$$\bar{N}_c(t) = [N_c(t) - N_c(0)]/[N_c(\infty) - N_c(0)]. \quad (3)$$

In the case of a free polymer and a central pinned system $n = 5$ ($X = N/2$), a sharp and monotonic rise in the $\bar{N}_c$ versus t curve is obtained, showing an all-or-none cluster formation in the system. When X is shifted towards the end of the chain, the steep-rise behavior vanishes. Instead, effective two-step kinetics is observed, and thus the associated two characteristic rates of the reaction can be defined. For $n = 1$, 2, and 3, one can notice an apparent plateau in $\bar{N}_c(t)$ plots, separating the two-time regimes. For these n values, the pinned monomer

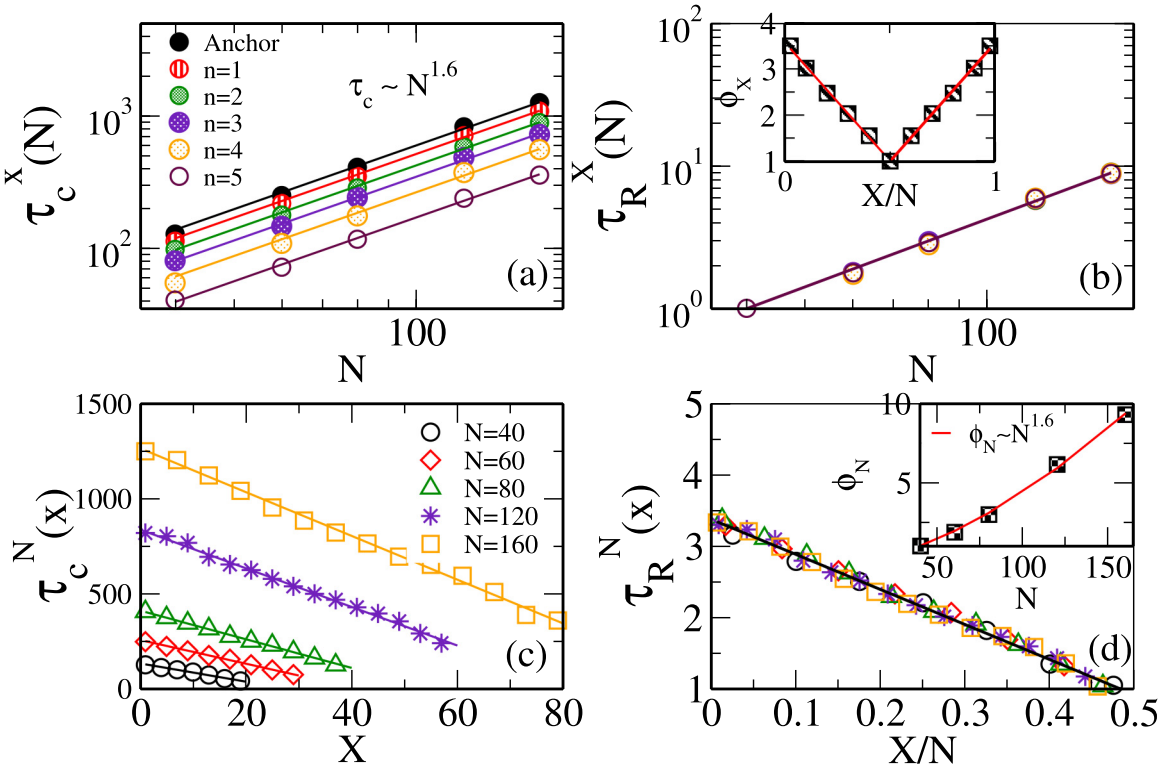

FIG. 7. Scaling behavior of collapse times (a) $\tau_c^X(N)$ vs N for fixed X, and (c) $\tau_c^N(X)$ vs X for fixed N [see Eq. (5)]. In plots (b) and (d), we show data collapse corresponding to (a) and (c), respectively, by plotting rescaled times $\tau_R^N(X)$ and $\tau_R^X(N)$ as defined in Eq. (5). Markers show the data point, and solid lines represent the fit $\tau_c \sim N^{1.60\pm0.03}$ [in (a)] and a linear fit [in (c)]. The multiplying factors ϕ_X and ϕ_N [see Eq. (6)] are shown in the inset of (b) and (d). In inset (b), solid lines represent a linear fit $\phi_X = a_0(X/N) + b_0$, $a_0 = \pm 5.1$.

divides the chain into two parts with unequal entropy. The initial rise indicates a fast accumulation of beads around the pinned monomer from the shorter end. The initial rise is followed by a wide plateau. After a certain time, a second—relatively faster—rise is obtained, representing the region where clusters of various sizes are activated along with both segments. The wide plateau shows that once a compact globule consisting of all the monomers from the shorter end is formed [the stage shown in Fig. 3(g)], the system waits until the longer segment overcomes the crumpling process. After that, the final coarsening starts [the stage shown in Fig. 3(h)], and a compact globule structure is formed.

V. COLLAPSE TIME τ_c

The total collapse time τ_c is defined as the time required for the $\langle R_g \rangle$ to reach 99% of its initial value during the transition from a coil state to the compact globule. Operationally, the duration of the collapse transition τ_c can be calculated from the equation [15,18,55]

$$R_g(\tau_c) = \tfrac{1}{100}[R_g(t=0) - \langle R_g \rangle_{\rm eq}] + \langle R_g \rangle_{\rm eq}. \tag{4}$$

From $\langle R_g \rangle_{\rm eq}$ and $\langle R_g(t) \rangle$ values given in Figs. 2, 4, and 5, we analyzed the collapsed time τ_c as a function of both parameters, i.e., the chain length N and the pinning index X. First we calculated $\tau_c(N)$ for a free polymer, presented in the inset of Fig. 4. The τ_c versus N curve for a free polymer satisfies a power law, and a relation $\tau_c \sim N^{1.60\pm0.03}$ is obtained by numerically fitting the calculated data shown in Fig. 4 (inset). For a free polymer, the value of the exponent is lower than the value predicted by Flory ($\tau_c \sim N^2$) and higher than $\tau_c \sim N^{1.01}$ obtained by Pham *et al.* [15] using Brownian dynamics simulations similar to ours. It is pertinent to note here that in the earlier studies, the initial configuration of a chain (at $t = 0$) was prepared by equilibrating it for a sufficiently long time in swollen state conditions; however, in our case we are starting from a stretched state configuration to avoid any crumple formation earlier than $t = 0$, which yields a larger timescale than the previous studies.

In Figs. 7(a) and 7(c), we have plotted $\tau_c^X(N)$ and $\tau_c^N(X)$, respectively. $\tau_c^X(N)$ represents the collapse time as a function of N when X is held fixed and $\tau_c^N(X)$ shows the collapse time as a function of X with fixed N. In Fig. 7(a), the τ_c versus N plot for the anchored polymer ($X = 1$) lies at the top, followed by the plots for $n = 2$, 3, and 4 with $n = 5$ ($X = N/2$) at the bottom. Interestingly, the collapse time follows the same scaling law as $\tau_c \sim N^{1.6}$ with the chain length N, independent of the pinning position X. In Fig. 7(c), the effect of pinning can be seen as τ_c decreases linearly with X. Again, for $N = 160$, time is maximum and minimum for $N = 40$ for all X values. In Figs. 7(b) and 7(d), we show a data collapse by rescaling the collapse times plotted in Figs. 7(a) and 7(c) using the following equations:

$$\begin{aligned} \tau_R^X(N) &= \tau_c^X(N)/\tau_c^X(40), \\ \tau_R^N(X) &= \tau_c^N(X)/\tau_c^N(\text{free}), \end{aligned} \tag{5}$$

where $\tau_c^X(40)$ is the collapse time of a chain length of $N = 40$ for each pinning position X. Similarly in Fig. 7(c), τ_{free}^N denotes the collapse time of a free polymer chain of corresponding length.

The nonsaturating trend in τ_c plots [see Fig. 7(c)] with X while reaching the center of the chain is not something that has been anticipated. It implies that the slightest shift in X (from the center) can influence τ_c and yield a timescale larger than the free polymer. We define this multiplying factor by the dimensionless quantities ϕ_X and ϕ_N, which measure the shift in timescales relative to the reference timescales. ϕ_X and ϕ_N are calculated as

$$\begin{aligned} \phi_X &= \tau_c^X(40)/\tau_c^{\text{free}}(40), \\ \phi_N &= \tau_c^N(\text{free})/\tau_c^{40}(\text{free}), \end{aligned} \tag{6}$$

where $\tau_c^{\text{free}}(40)$ is the collapse time of a free chain of length $N = 40$, however ϕ_X does not change if calculated using different N values (other than $N = 40$). ϕ_X quantifies the difference in timescales for different pinning positions quite adequately in Fig. 7(b) (inset). Interestingly, the plot suggests that irrespective of the chain length, τ_c for the anchored polymer remains nearly four times larger than the τ_c for the central pinned polymer.

Similarly, ϕ_N is plotted against N in Fig. 7(d) (inset) to measure the difference in timescales between different chain lengths as a constant value of X. As expected, ϕ_N follows the same scaling $\sim N^{1.6}$ as the τ_c. The observed data collapse is pretty good, which implies that for every pinning position X, τ_c will follow the same scaling law as the free polymer.

Using $\tau_c(N)$ values, we show data collapse for $\bar{N}_c(t)$ of different lengths as a function of re-scaled time t/τ_c on a log-log plot [see Fig. 8(a)]. As reported in Refs. [12,15,18], the log-log plots show power-law behavior for the average cluster size N_c growth with time as t^z, where z is defined as the collapse exponent. For a free or central pinned monomer, we obtain scaling exponents $z = 1.00 \pm 0.04$, which is identical to the value of z reported in Ref. [18]. Similar results were also obtained in the work of Pham *et al.* [15], however Byrne *et al.* [12] found an exponent value of $z = 0.66$.

In Figs. 8(b)–8(d), we show that z deviates from its value for the free polymer [Fig. 8(a)] significantly in the early time regime, while at longer times, it again scales with the same z value. These two regimes are separated with a clear plateau in all three cases, i.e., for the anchored case and the $n = 2$ and 3 cases (n is as defined in Figs. 5 and 6). We find $z = 0.75 \pm 0.04$, 0.88 ± 0.04, and 0.97 ± 0.03 for the anchored, $n = 2$, and $n = 3$ case, respectively, which shows that pinning a monomer close to the center drives the process faster, and vice versa. The difference in z values at early times corresponds to the fast accumulation of monomers from the shorter segment close to the pinned monomer; therefore, a first rise in $\bar{N}_c(t)$ plots is seen, whereas in the longer segment, crumpling is relatively slower. This time difference in the dynamics of both segments yields a plateau between the two time regimes. After the coarsening starts in the longer segments, $\bar{N}_c(t)$ plots register a second sharp rise with exponent value $z = 1$ independent of the X value. Notably, in the case of a free polymer, similar to a central pinned system, there is no entropy difference in both of the divided segments, thus the plateau vanishes.

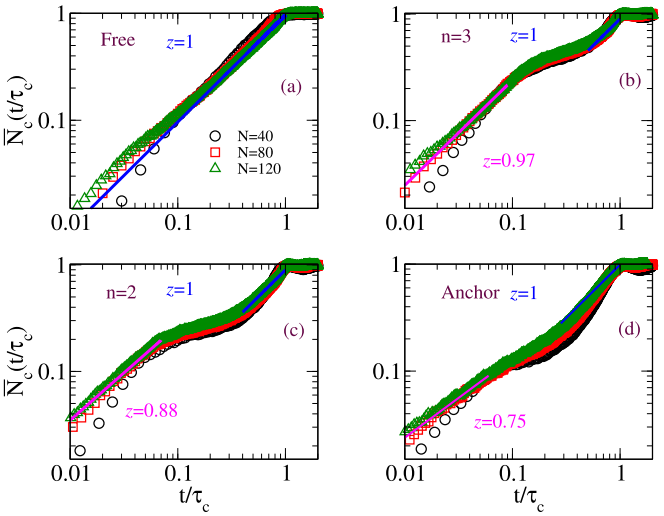

FIG. 8. Normalized $\bar{N}_c(t)$ vs t/τ_c on a log-log plot for (a) free polymer, (b) $n = 3$ ($X = 12$ for $N = 40$), (c) $n = 2$ ($X = 8$ for $N = 40$), and (d) anchored ($X = 1$). From plot (a), we obtained the value of collapse exponent $z = 1.00 \pm 0.04$, while after pinning a monomer [shown in plots (b)–(d)], we identified two different time regimes. The initial rise at early times corresponds to $z < 1$ values ($z = 0.97 \pm 0.03$ for $n = 3$, $z = 0.88 \pm 0.04$ and 0.75 ± 0.04 for anchor), while at longer times, we obtained $z = 1$. The errors bars are obtained using the method of least squares.

VI. CONCLUSION

In this paper, we present the kinetics of a collapsing pinned homopolymer using the Langevin dynamics simulation. At first, a free polymer chain of variable length ($N = 40$, 60, 80, 120, 160, and 240) is equilibrated for a sufficiently long time, and the temperature dependency of $\langle R_g \rangle$ is recorded. A crossover in $\langle R_g^2 \rangle / N$ plot is used to locate the T_θ point ($T = 3.4$, as obtained), below which the polymer is considered in a collapsed state irrespective of the chain length N. The kinetics of a free polymer is explained through the "pearl necklace" mechanism, which predominately involves an early, rapid formation of small clusters followed by the straightening of chain sections between the clusters and, lastly, the cluster coarsening, which creates the final globule structure. The growth of clusters in size satisfies $\bar{N}_c(t) \sim t^z$, where $z = 1.00 \pm 0.04$, and the collapse timescale as $\tau_c \sim N^{1.60 \pm 0.03}$, where N is the degree of polymerization. The scaling laws we obtained for a free polymer show good agreement with the previous studies.

In the next part, the collapse pathway of a polymer with a pinned monomer at a position $1 \leqslant X \leqslant N$ is investigated. We showed that the collapse time τ_c is sensitive to the change in pinning position, except for the case in which the central monomer is pinned ($X = N/2$). The calculated τ_c for the central pinned system is minimum and identical to the τ_c of a free polymer. Moving X from the center ($X = N/2$) to the end ($X = 1$ or N) of the chain causes the process to be delayed and

the total collapse time increases linearly with X. The reason for different timescales is the symmetry breaking caused by the frozen monomer, which divides the chain into two parts of unequal entropy.

We investigated the dependency of τ_c on X for various chain lengths. We found that the linear relation between τ_c and X values is novel and unaffected by any change in the polymer length. Interestingly, for every X, the same scaling law $\tau_c \sim N^{1.6}$ is obtained, as in the case of a free polymer. We define two dimensionless factors ϕ_X and ϕ_N, which quantify the joint effect of pinning position X and the degree of polymerization N on the collapse time τ_c. The total collapse time scales as $\tau_c \sim \phi_X N^{1.6}$ in pinned polymers, where ϕ_X incorporates the pinning effect on the dynamical timescales. In our simulation, we found that the time involved in the collapse of an anchored polymer is fourfold that of the free polymer, independent of the chain length N. The second factor scales with N as $\phi_N \sim N^{1.6}$, showing that the τ_c dependency on N is system-invariant.

By showing the cluster growth $\bar{N}_c$ as a function of rescale time t/τ_c, we argue that a stronger effect of pinning, in the form of two-step growth in cluster size, appears for certain X values. For these X values, a plateau separates an initial rise at early times from a second steep rise at longer times. At longer times, cluster growth follows the same scaling law for the pinned and free system $\bar{N}_c(t) \sim t^z$, where $z = 1.00 \pm 0.04$; however, the collapse coefficient $z \neq 1$ during the early times and attains a value depending on X. We obtained $z = 0.97 \pm 0.03$ for $n = 3$, $z = 0.88 \pm 0.04$ for $n = 2$, and $z = 0.75 \pm 0.04$ for an anchored polymer ($X = 1$ or N). We explain that the reason for different regimes is the fast aggregation of monomers from the shorter segment around the pinned monomer, while the longer chain is limited to slow crumpling at these times, and the system waits for the final coarsening to start. For the symmetric cases $X = N/2$ and the free polymer, there is no lag present between the folding of the two segments, the plateau vanishes, and a single step growth is obtained.

ACKNOWLEDGMENTS

We thank the anonymous referees for several suggestions that have greatly improved the presentation of the paper. We are grateful to Yashwant Singh and Sanjay Kumar for their constant encouragement and support during the preparation of this work, and also for providing us with the computational facility for performing the simulations. K.C. and A.S. would like to thank DST-Inspire (India) and CSIR (India) for providing financial assistance.

[1] B. Alberts, A. Johnson, J. Lewis, D. Morgan, M. Raff, K. Roberts, P. Walter, J. Wilson, and T. Hunt, *Molecular Biology of the Cell* (WW Norton & Co., New York, 2017).
[2] W. Stockmayer, Problems of the statistical thermodynamics of dilute polymer solutions, Makromol. Chem. **35**, 54 (1960).
[3] P. Flory and W. Krigbaum, Statistical mechanics of dilute polymer solutions. ii, J. Chem. Phys. **18**, 1086 (1950).
[4] P. G. de Gennes, *Scaling Concepts in Polymer Physics* (Cornell University, Ithaca, 1979).
[5] P. G. de Gennes, Kinetics of collapse for a flexible coil, J. Phys. Lett. **46**, 639 (1985).
[6] J. Xu, Z. Zhu, S. Luo, C. Wu, and S. Liu, First Observation of Two-Stage Collapsing Kinetics of a Single Synthetic Polymer Chain, Phys. Rev. Lett. **96**, 027802 (2006).
[7] A. Halperin and P. M. Goldbart, Early stages of homopolymer collapse, Phys. Rev. E **61**, 565 (2000).
[8] F. Ganazzoli, R. La Ferla, and G. Allegra, Kinetics of contraction of a stiff chain, Macromolecules **28**, 5285 (1995).
[9] D. Thirumalai, From minimal models to real proteins: time scales for protein folding kinetics, J. Phys. I (Paris) **5**, 1457 (1995).
[10] L. Klushin, Kinetics of a homopolymer collapse: beyond the rouse–zimm scaling, J. Chem. Phys. **108**, 7917 (1998).
[11] T. Kavassalis and P. Sundararajan, A molecular-dynamics study of polyethylene crystallization, Macromolecules **26**, 4144 (1993).
[12] A. Byrne, P. Kiernan, D. Green, and K. A. Dawson, Kinetics of homopolymer collapse, J. Chem. Phys. **102**, 573 (1995).
[13] G. Tanaka and W. L. Mattice, Chain collapse by atomistic simulation, Macromolecules **28**, 1049 (1995).
[14] C. Liu, K. Kubo, E. Wang, K.-S. Han, F. Yang, G. Chen, F. A. Escobedo, G. W. Coates, and P. Chen, Single polymer growth dynamics, Science **358**, 352 (2017).
[15] T. T. Pham, M. Bajaj, and J. R. Prakash, Brownian dynamics simulation of polymer collapse in a poor solvent: influence of implicit hydrodynamic interactions, Soft Matter **4**, 1196 (2008).
[16] N. Kikuchi, J. F. Ryder, C. M. Pooley, and J. M. Yeomans, Kinetics of the polymer collapse transition: the role of hydrodynamics, Phys. Rev. E **71**, 061804 (2005).
[17] E. Pitard, Influence of hydrodynamics on the dynamics of a homopolymer, Eur. Phys. J. B **7**, 665 (1999).
[18] J. Guo, H. Liang, and Z.-G. Wang, Coil-to-globule transition by dissipative particle dynamics simulation, J. Chem. Phys. **134**, 244904 (2011).
[19] J. M. Polson and N. E. Moore, Simulation study of the coil-globule transition of a polymer in solvent, J. Chem. Phys. **122**, 024905 (2005).
[20] P. Español and P. B. Warren, Perspective: Dissipative particle dynamics, J. Chem. Phys. **146**, 150901 (2017).
[21] S. Majumder and W. Janke, Cluster coarsening during polymer collapse: Finite-size scaling analysis, Europhys. Lett. **110**, 58001 (2015).
[22] S. Ghosh and S. Vemparala, Kinetics of charged polymer collapse in poor solvents, J. Phys.: Condens. Matter **34**, 045101 (2022).
[23] F. L. McCrackin, J. Mazur, and C. M. Guttman, Monte Carlo studies of self-interacting polymer chains with excluded volume. i. squared radii of gyration and mean-square end-to-end distances and their moments, Macromolecules **6**, 859 (1973).
[24] M. Cieśla, J. Pawłowicz, and L. Longa, Molecular dynamics simulation of the lennard-jones polymers in a good solvent, Acta Phys. Polon. B **38**, 1727 (2007).

[25] L. Léger, E. Raphaël, and H. Hervet, Surface-anchored polymer chains: Their role in adhesion and friction, in *Polymers in Confined Environments* (Springer, Berlin, Heidelberg, 1999), vol. 138, pp. 185–225.

[26] S. Kumar, K. Chauhan, S. Singh, and D. Foster, Polymer in wedge-shaped confinement: Effect on the θ temperature, Phys. Rev. E **101**, 030502(R) (2020).

[27] D. Mohanta, Melting of confined dna: static and dynamic properties, Soft Matter **18**, 2790 (2022).

[28] R. H. Levi, Y. Kantor, and M. Kardar, Pinning and unbinding of ideal polymers from a wedge corner, Phys. Rev. E **96**, 062132 (2017).

[29] S. Chakrabarty, R. Das, S. Karmakar, and C. Dasgupta, Understanding the dynamics of glass-forming liquids with random pinning within the random first order transition theory, J. Chem. Phys. **145**, 034507 (2016).

[30] M. Ozawa, W. Kob, A. Ikeda, and K. Miyazaki, Equilibrium phase diagram of a randomly pinned glass-former, Proc. Natl. Acad. Sci. (USA) **112**, 6914 (2015).

[31] C. Cammarota and G. Biroli, Random pinning glass transition: Hallmarks, mean-field theory and renormalization group analysis, J. Chem. Phys. **138**, 12A547 (2013).

[32] S. Gokhale, K. H. Nagamanasa, R. Ganapathy, and A. Sood, Growing dynamical facilitation on approaching the random pinning colloidal glass transition, Nat. Commun. **5**, 4685 (2014).

[33] A. Singh and Y. Singh, Super-Arrhenius behavior of molecular glass formers, Phys. Rev. E **99**, 030101(R) (2019).

[34] A. Singh, S. M. Bhattacharyya, and Y. Singh, Emergence of cooperatively reorganizing cluster and super-Arrhenius dynamics of fragile supercooled liquids, Phys. Rev. E **103**, 032611 (2021).

[35] C. Cammarota, A general approach to systems with randomly pinned particles: Unfolding and clarifying the random pinning glass transition, Europhys. Lett. **101**, 56001 (2013).

[36] U. K. Nandi, P. Patel, M. Moid, M. K. Nandi, S. Sengupta, S. Karmakar, P. K. Maiti, C. Dasgupta, and S. Maitra Bhattacharyya, Thermodynamics and its correlation with dynamics in a mean-field model and pinned systems: A comparative study using two different methods of entropy calculation, J. Chem. Phys. **156**, 014503 (2022).

[37] T. Wu *et al.*, Spin pinning effect to reconstructed oxyhydroxide layer on ferromagnetic oxides for enhanced water oxidation, Nat. Commun. **12**, 3634 (2021).

[38] K. S. Alexander and V. Sidoravicius, Pinning of polymers and interfaces by random potentials, Ann. Appl. Probab. **16**, 636 (2006).

[39] W. Huang and V. Zaburdaev, The shape of pinned forced polymer loops, Soft Matter **15**, 1785 (2019).

[40] C. C. Chow and J. J. Collins, Pinned polymer model of posture control, Phys. Rev. E **52**, 907 (1995).

[41] L.-Z. Sun, W.-P. Cao, and M.-B. Luo, Free energy landscape for the translocation of polymer through an interacting pore, J. Chem. Phys. **131**, 194904 (2009).

[42] K. Chauhan and S. Kumar, Dynamics of a polymer chain translocating through varying cone-shaped channels, Phys. Rev. E **103**, 042501 (2021).

[43] J. E. Moisio, J. Piili, and R. P. Linna, Driven polymer translocation in good and bad solvent: Effects of hydrodynamics and tension propagation, Phys. Rev. E **94**, 022501 (2016).

[44] R. K. Mishra, G. Mishra, D. Giri, and S. Kumar, Scaling of hysteresis loop of interacting polymers under a periodic force, J. Chem. Phys. **138**, 244905 (2013).

[45] K. Chauhan, A. R. Singh, S. Kumar, and R. Granek, Can one detect intermediate denaturation states of dna sequences by following the equilibrium open–close dynamic fluctuations of a single base pair? J. Chem. Phys. **156**, 164907 (2022).

[46] T. Pal, K. Chauhan, and S. Kumar, Role of Hoogsteen interaction in the stability of different phases of triplex DNA, Phys. Rev. E **105**, 044407 (2022).

[47] S. M. Bhattacharjee, A. Giacometti, and A. Maritan, Flory theory for polymers, J. Phys.: Condens. Matter **25**, 503101 (2013).

[48] B. M. Baysal and F. E. Karasz, Coil-globule collapse in flexible macromolecules, Macromol. Theor. Simul. **12**, 627 (2003).

[49] P. Grassberger and R. Hegger, Simulations of three-dimensional θ polymers, J. Chem. Phys. **102**, 6881 (1995).

[50] S. Majumder, J. Zierenberg, and W. Janke, Kinetics of polymer collapse: effect of temperature on cluster growth and aging, Soft Matter **13**, 1276 (2017).

[51] T. Vogel, M. Bachmann, and W. Janke, Freezing and collapse of flexible polymers on regular lattices in three dimensions, Phys. Rev. E **76**, 061803 (2007).

[52] J. Suzuki, A. Takano, and Y. Matsushita, The theta-temperature depression caused by topological effect in ring polymers studied by monte carlo simulation, J. Chem. Phys. **135**, 204903 (2011).

[53] M. N. Chernodub, M. Lundgren, and A. J. Niemi, Elastic energy and phase structure in a continuous spin Ising chain with applications to chiral homopolymers, Phys. Rev. E **83**, 011126 (2011).

[54] S. Das, N. Kennedy, and A. Cacciuto, The coil–globule transition in self-avoiding active polymers, Soft Matter **17**, 160 (2021).

[55] Y. A. Kuznetsov, E. G. Timoshenko, and K. A. Dawson, Kinetic laws at the collapse transition of a homopolymer, J. Chem. Phys. **104**, 3338 (1996).